The entanglement properties of holographic QCD model with a critical end point*

Zhibin Li(李志镔)[1†] Kun Xu(许坤)[2,3‡] Mei Huang(黄梅)[2§]

[1]School of Physics, Zhengzhou University, No.100 Science Avenue, Zhengzhou 450001, China
[2]School of Nuclear Science and Technology, University of Chinese Academy of Sciences, Beijing 100049, China
[3]Institute of High Energy Physics, Chinese Academy of Sciences, Beijing 100049, China

Abstract: We investigated different entanglement properties of a holographic QCD (hQCD) model with a critical end point at the finite baryon density. Firstly, we considered the holographic entanglement entropy (HEE) of this hQCD model in a spherical shaped region and a strip shaped region. It was determined that the HEE of this hQCD model in both regions can reflect QCD phase transition. Moreover, although the area formulas and minimal area equations of the two regions were quite different, the HEE exhibited a similar behavior on the QCD phase diagram. Therefore, we assert that the behavior of the HEE on the QCD phase diagram is independent of the shape of the subregions. However, the HEE is not an ideal parameter for the characterization of the entanglement between different subregions of a thermal system. As such, we investigated the mutual information (MI), conditional mutual information (CMI), and the entanglement of purification (Ep) in different strip shaped regions. We determined that the three entanglement quantities exhibited some universal behavior; their values did not change significantly in the hadronic matter phase but increased rapidly with the increase in T and μ in the QGP phase. Near the phase boundary, these three entanglement quantities changed smoothly in the crossover region and continuously but not smoothly at CEP; they exhibited discontinuous behavior in the first phase transition region. These properties can be used to distinguish between the different phases of strongly coupled matter.

Keywords: holographic QCD, critical end point, entanglement properties

DOI: 10.1088/1674-1137/abc539

I. INTRODUCTION

Entanglement plays a very important role in a strongly coupled system. In a quantum many body system, entanglement entropy is a measurement of quantum correlation between different parts of the system [1]. In the case of AdS/CFT correspondence or more general Gauge/Gravity duality [2-5], the holographic entanglement entropy provides insights into quantum information and quantum gravity [6-10].

From quantum field theory, e.g., quantum chromodynamics (QCD), the entire system is represented in 4-dimensional Minkowski spacetime, and for any state at a fixed time t_0, we have the state vector $|\Psi(t_0)\rangle$ and the density matrix given as

$$\rho = |\Psi(t_0)\rangle\langle\Psi(t_0)|. \tag{1}$$

To investigate the entanglement entropy between different parts of this system, we first divide the entire time slice into two parts, which we denote as A and $\bar{A}$, where A is a subregion of the time slice and $\bar{A}$ is its complement. We then obtain the reduced density matrix of the subsystem A by tracing out the degree of freedom of subsystem $\bar{A}$ in the Hilbert space

$$\rho_A = \mathrm{tr}_{\bar{A}}\rho. \tag{2}$$

The entanglement entropy of subsystem A can be defined as the von Neumann entropy [1]

Received 9 August 2020; Accepted 29 September 2020; Published online 24 November 2020

* Z.L. acknowledge support by the NSFC (11947233), CPSF (2019M662507) and the start-up funding from Zhengzhou University. The work of M.H. was supported in part by the NSFC (11725523, 11735007, 11261130311) (CRC 110 by DFG and NSFC), Chinese Academy of Sciences (XDPB09), the Fundamental Research Funds for the Central Universities and the start-up funding from University of Chinese Academy of Sciences

† E-mail: lizhibin@zzu.edu.cn
‡ E-mail: xukun@ihep.ac.cn
§ E-mail: huangmei@ucas.ac.cn

$$S_A = -\mathrm{tr}(\rho_A \log \rho_A). \tag{3}$$

However, it is not easy to directly calculate the entanglement entropy in the QCD side using this formula. According to the AdS/CFT correspondence or AdS/QCD correspondence [5, 11-14] we know that the holographic duality of the entanglement entropy between boundary region A and its complement is the holographic entanglement entropy which can be calculated using the Ryu-Takayanagi formula [15, 16] as follows:

$$\begin{aligned} S_A \equiv S_A^h &= \frac{\mathrm{Area}(\min_{m(A)\sim A}\{m(A)\})}{4G_N} \\ &= \frac{\mathrm{Area}(\gamma_A)}{4G_N} = \frac{2\pi}{\kappa^2}\mathrm{Area}(\gamma_A), \end{aligned} \tag{4}$$

where $m(A)$ is a 3-dimensional surface in the bulk which is homologous to A. The holographic entanglement entropy is equal to the minimal area $m(A)$, which is denoted as γ_A (the R-T surface) divided by a constant $4G_N$. There have been several studies on the relationship between the holographic entanglement properties and the phase transition in holographic QCD models [17-22]. In a previously published report [17], the behavior of holographic entanglement entropy with temperature at the zero baryon chemical potential was investigated. In a separate study [18], the authors investigated holographic entanglement entropy in a strip shaped region in a holographic QCD model. Both studies determined that holographic entanglement entropy is sensitive to the phase transition of QCD matter.

Another very important aspect of holographic entanglement entropy is the shape dependence of the subregion A [23-25]. Since QCD theory applies to 4-dimensional spacetime, it is very difficult to calculate the holographic entanglement entropy for a general shaped region A. Therefore, we consider two different shapes in our work to study the shape dependence of region A. One is a spherical shaped region and the other is a strip shaped region.

For a thermal system with finite temperature T and chemical potential μ, entanglement entropy is not a reliable parameter for the measurement of the entanglement between different subsystems because of the thermodynamic contributions. To further elaborate on this concept, let us consider the purification of the quantum state on the boundary of a Schwarzschild-AdS black hole. It has been shown that the purified state lives on the double boundary of the bulk spacetime, which can be denoted as B and $\bar{B}$. If we divide B into two disjointed subregions A and $\bar{A}$, the holographic entanglement entropy of subregion A measures the entanglement between A and its complement $\bar{A}\cup\bar{B}$ (but not $\bar{A}$) [26]. By using the subadditivity and strong subadditivity of entanglement entropy, one can define two nonnegative entanglement quantities, the mutual information $MI(A,B)$ and conditional mutual information $CMI(A,B|C)$, as [15, 16]

$$MI(A,B) = S(A) + S(B) - S(AB), \tag{5}$$

$$CMI(A,B|C) = S(AC) + S(BC) - S(ABC) - S(C). \tag{6}$$

It is believed that mutual information and conditional mutual information are better quantities for the measurement of the entanglement between different subsystems of a thermal system, compared to the entanglement entropy. However, these two quantities are simply the linear combination of entanglement entropy and not new quantities that describe entanglement in a thermal state. In recent years, a new entanglement quantity based on the purification of the thermal state, called the entanglement of purification (Ep), has been investigated [27-31]. For a thermal state on the boundary time slice, two unintersected subsystems A and B chosen on the thermal state ρ_{AB} can be purified as

$$\rho_{AB} = Tr_{A^*B^*}(|\sqrt{\rho}\rangle\langle\sqrt{\rho}|), \tag{7}$$

where $|\sqrt{\rho}\rangle\langle\sqrt{\rho}| = \rho$ is a pure state density matrix. Then, the entanglement of purification for A and B can be defined as [32]

$$Ep(A,B) = \min_{\rho_{AB}=Tr_{A^*B^*}(|\sqrt{\rho}\rangle\langle\sqrt{\rho}|)} S(\rho_{AA^*}), \tag{8}$$

where $\rho_{AA^*}=Tr_{BB^*}(|\sqrt{\rho}\rangle\langle\sqrt{\rho}|)$, and $S(\rho_{AA^*})$ is the entanglement entropy associated with ρ_{AA^*}. It is difficult to determine the appropriate purification for a general ρ_{AB} for the field theory side. The holographic duality of Ep is believed to be the entanglement wedge cross section [27]

$$Ep(A,B) = Ew(A,B) = \frac{\mathrm{Area}(\Sigma_{AB}^{\min})}{4G_N}, \tag{9}$$

where $\Sigma_{AB}^{\min}$ is the minimal surface area in the entanglement wedge of A and B that ends on their R-T surface, as shown in Fig. 12. The blue regions are the subregions A and B , and the red surfaces are the R-T surfaces of $A\cup B$. The green surface is the minimal surface $\Sigma_{AB}^{\min}$.

The remainder of this report is arranged as follows. In section II, we describe the model setting used in this work. In section III, we initially analytically compute the holographic entanglement entropy and derive the minimal area equations. We then analyze the numerical results for holographic entanglement entropy and compare it to the black hole entropy. We also investigate the behavior

of other entanglement quantities such as mutual information, conditional mutual information, and entanglement of purification on the phase diagram in section IV. Finally, the conclusion and discussion are presented in section V.

II. HOLOGRAPHIC QCD MODEL

The holographic QCD model we consider in this work is a 5-dimensional Einstein-Maxwell-dilaton holographic model, which is described as follows [33]:

$$S=\frac{1}{2\kappa^2}\int \mathrm{d}^5x\sqrt{-g}\left[R-\frac{f(\phi)}{4}F_{\mu\nu}^2-\frac{1}{2}(\partial\phi)^2-V(\phi)\right], \quad (10)$$

where κ^2 is the gravitational constant, and $\kappa^2=8\pi G_N$; g is the determinant of the 5-dimensional metric $g_{\alpha\beta}$. The first term R is the Ricci scalar, which corresponds to the QCD vacuum sector. The scalar field, ϕ, corresponds to the gluon scalar condensate, and $F_{\mu\nu}:=\partial_\mu A_\nu-\partial_\nu A_\mu$ is the strength tensor of a $U(1)$ gauge field A_μ, which gives the quark chemical potential and density. We then take the ansatz of the asymptotic AdS_5 metric as follows [33]:

$$\mathrm{d}s^2=\frac{\mathrm{e}^{2A_e(z)}}{z^2}\left[-\chi(z)\mathrm{d}t^2+\frac{1}{\chi(z)}\mathrm{d}z^2+\mathrm{d}\vec{x}^2\right], \quad (11)$$

where z is the holographic direction of the asymptotic AdS_5, and $z=0$ corresponds to the ultra-violet (UV) boundary spacetime for which the QCD theory is applicable. Following [33], the dilaton field and the gauge field take the forms of

$$\phi\equiv\phi(z), \quad A_\mu\mathrm{d}x^\mu\equiv A_t(z)\mathrm{d}t. \quad (12)$$

Using the regular boundary conditions at the horizon $z=z_H$ and the asymptotic AdS_5 conditions at the UV boundary $z=0$ [33], we have

$$A_t(z_H)=\chi(z_H)=0, \quad (13)$$

$$A(0)=-\sqrt{\frac{1}{6}}\phi(0), \quad \chi(0)=1, \quad (14)$$

$$A_t(0)=\frac{1}{3}\mu+3\rho z^2+\cdots, \quad (15)$$

where μ and ρ are the baryon chemical potential and density, respectively. The warped factor and gauge kinetic function can be fixed as [33]

$$A_e(z)=-\frac{c}{3}z^2-bz^4, \quad (16)$$

$$f(\phi(z))=\mathrm{e}^{cz^2-A_e(z)}. \quad (17)$$

By solving the equation of motion we get [33]

$$\begin{aligned}\chi(z)=1+&\frac{1}{\int_0^{z_H}\mathrm{e}^{-3A_e(y)}\mathrm{d}y}\left\{\frac{2c\mu^2}{(1-\mathrm{e}^{cz_H^2})^2}\left[\int_0^{z_H}\mathrm{e}^{-3A_e(y)}\mathrm{d}y\right.\right.\\&\times\int_{z_H}^{z}\mathrm{e}^{cy^2-3A_e(y)}\mathrm{d}y-\int_0^{z_H}\mathrm{e}^{cy^2-3A_e(y)}\mathrm{d}y\int_{z_H}^{z}\mathrm{e}^{-3A_e(y)}\mathrm{d}y\left.\right]\\&\left.-\int_0^{z}\mathrm{e}^{-3A_e(y)}\mathrm{d}y\right\}.\end{aligned} \quad (18)$$

We can also calculate the baryon density ρ and the temperature T as [33]

$$\rho=\frac{c\mu}{9(1-\mathrm{e}^{cz_H^2})}, \quad (19)$$

$$\begin{aligned}T=&\frac{z_H^3\mathrm{e}^{-3A_e(z_H)}}{4\pi\int_0^{z_H}y^3\mathrm{e}^{-3A_e(y)}\mathrm{d}y}\\&\times\left[1-\frac{2c\mu^2\left(\mathrm{e}^{cz_H^2}\int_0^{z_H}y^3\mathrm{e}^{-3A_e(y)}\mathrm{d}y-\int_0^{z_H}y^3\mathrm{e}^{cy^2-3A_e(y)}\mathrm{d}y\right)}{9\left(1-\mathrm{e}^{cz_H^2}\right)^2}\right].\end{aligned} \quad (20)$$

Then, by fitting the vacuum vector meson mass $m_\rho=0.77$ GeV and the phase transition temperature $T_c=0.17$ GeV at $\mu=0$, we can fix c and b as in [33]:

$$b=-6.25\times10^{-4}\ \mathrm{GeV}^4, \quad c=0.227\ \mathrm{GeV}^2. \quad (21)$$

Based on the preceding parameters, the phase diagram for deconfined phase transition of the holographic QCD model of [33] is shown in Fig. 1.

The dashed line is the phase boundary of the crossover region ($\mu<0.693$ GeV), the blue dot is the CEP located at ($\mu^E=0.693$ GeV, $T^E=0.121$ GeV), and the solid line is the first order phase boundary ($\mu>0.693$ GeV). The black hole entropy of this system can be derived as:

$$S_{bh}=\frac{2\pi}{\kappa^2}\frac{\mathrm{e}^{3A_e(z_H)}}{z_H^3}\int_{-\infty}^{\infty}\mathrm{d}x_1\int_{-\infty}^{\infty}\mathrm{d}x_2\int_{-\infty}^{\infty}\mathrm{d}x_3. \quad (22)$$

It is evident that this black hole entropy is divergent. However, given that we need to determine the relationship between the temperature, T, and baryon chemical potential, μ, of the black hole entropy, we can exclude the divergent part and define the entropy density as follows:

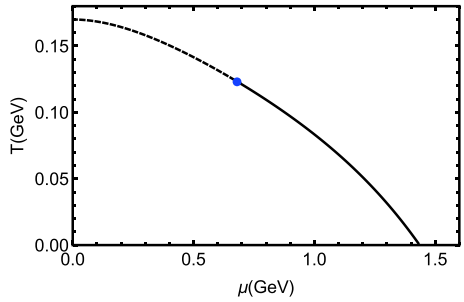

Fig. 1. The phase diagram of the holographic QCD model used in this work [33]. The dashed line is the phase boundary of the crossover region ($\mu < 0.693$ GeV), the blue dot is the CEP located at ($\mu^E = 0.693$ GeV, $T^E = 0.121$ GeV), and the solid line is the first order phase boundary ($\mu > 0.693$ GeV).

$$s_{bh} = \frac{2\pi}{\kappa^2}\frac{e^{3A_e(z_H)}}{z_H^3}. \tag{23}$$

III. HOLOGRAPHIC ENTANGLEMENT ENTROPY

In this section, we will consider the holographic entanglement entropy in the holographic QCD model that was defined in the last section. In this work, we choose the subregion A to be highly symmetric: 1) a spherically-shaped region on the boundary time slice with $0 \leqslant \vec{x}^2 \leqslant r_0^2$ is shown in Fig. 2; 2) a strip-shaped region on the boundary time slice with $-a/2 \leqslant x_1 \leqslant a/2$ and $-\infty < x_i < \infty$ for $i = 2,3$ is shown in Fig. 3. The blue region is region A, and the red region is the surface, γ_A ,which is the minimal surface that is homologous to A in the bulk. It will be very convenient to transform to spherical coordinates for the spherical shaped region A, for which this region will be $0 < r < r_0$, as represented by the blue line in Fig. 2 , and the red line is the minimal surface, γ_A.

A. Minimal area equation

For a spherical shaped region A shown in Fig. 2, the area of $m(A)$ with $m(A) : z = z(x_1, x_2, x_3)$ is given by

$$\begin{aligned}\text{Area}(m(A)) &= \int_A \sqrt{h}\mathrm{d}x_1\mathrm{d}x_2\mathrm{d}x_3 = \int_A \frac{e^{3A_e(z)}}{z^3} \\ &\times \sqrt{1+\frac{(\partial_{x_1}z)^2+(\partial_{x_2}z)^2+(\partial_{x_3}z)^2}{\chi(z)}}\mathrm{d}x_1\mathrm{d}x_2\mathrm{d}x_3,\end{aligned} \tag{24}$$

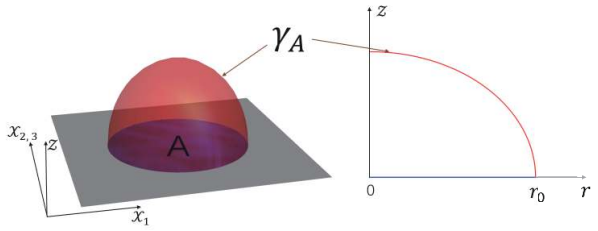

Fig. 2. (color online) (Left) The spherical shaped subregion A (the blue region) and the minimal surface, γ_A, (the red surface). (Right) In spherical coordinates, we only need to consider the direction of the radius. Region A is from $r = 0$ to $r = r_0$ and the minimal surface, γ_A , can be determined by $z = z(r)$, which is the solution of the minimal area equation.

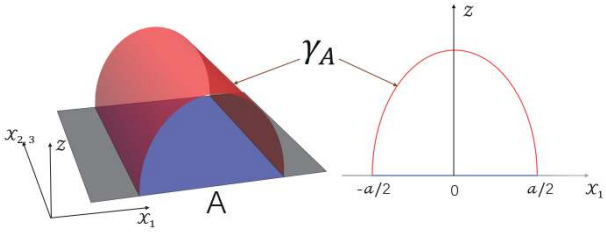

Fig. 3. (color online) (Left) The strip shaped subregion A (the blue region) and the minimal surface, γ_A, (the red surface). (Right) Given the symmetry of region A, we only need to consider the x_1 direction, and this region is defined by $-a/2 < x_1 < a/2$ (the blue line) . The minimal surface, γ_A, is determined by $z = z(x_1)$, which is the solution of the minimal area equation.

where h is the determinant of the reduced metric on surface $m(A)$. After transforming to spherical coordinates, we have $z = z(r,\theta,\phi)$. We then exploit the symmetry of region A and the bulk time slice since the minimal surface should have the same symmetry with A. This means that we only need to consider surfaces defined by $z = z(r)$ as shown in Fig. 2. Thus, we have

$$\begin{aligned}\text{Area}(m(A)) &= \int_0^{r_0} r^2\mathrm{d}r\int_0^{\pi}\sin(\theta)\mathrm{d}\theta\int_0^{2\pi}\mathrm{d}\phi\frac{e^{3A_e(z)}}{z^3}\sqrt{1+\frac{(\partial_r z)^2}{\chi(z)}} \\ &= 4\pi\int_0^{r_0} r^2\mathrm{d}r\frac{e^{3A_e(z)}}{z^3}\sqrt{1+\frac{(\partial_r z)^2}{\chi(z)}}.\end{aligned} \tag{25}$$

The minimal area equation can be calculated as

$$\partial_r^2 z - \frac{2\left[\chi(z)+(\partial_r z)^2\right]\left[3r\chi(z)(z\partial_z A_e(z)-1)-2z\partial_r z\right]+rz\partial_z\chi(z)(\partial_r z)^2}{2rz\chi(z)} = 0, \tag{26}$$

with the boundary conditions

$$z(r_0)=0, \quad \partial_r z(r)|_{r=0}=0, \tag{27}$$

we can solve the minimal area equation with the solution $z=z_m(r)$. Then, the area of the minimal surface is given by

$$\text{Area}(\gamma_A)=4\pi\int_0^{r_0} r^2\mathrm{d}r\frac{\mathrm{e}^{3A_e(z_m)}}{z_m^3}\sqrt{1+\frac{(\partial_r z_m)^2}{\chi(z_m)}}, \tag{28}$$

and the holographic entanglement entropy for a spherical shaped region is given as

$$S_A^{sp}=\frac{2\pi}{\kappa^2}\text{Area}(\gamma_A)=\frac{8\pi^2}{\kappa^2}\int_0^{r_0} r^2\mathrm{d}r\frac{\mathrm{e}^{3A_e(z_m)}}{z_m^3}\sqrt{1+\frac{(\partial_r z_m)^2}{\chi(z_m)}}. \tag{29}$$

For a strip shaped region A, as shown in Fig. 3, the area of surface $m(A)$ is

$$\text{Area}(m(A))=\int_A\sqrt{h}\mathrm{d}x_1\mathrm{d}x_2\mathrm{d}x_3=\int_A\frac{\mathrm{e}^{3A_e(z)}}{z^3}\times\sqrt{1+\frac{(\partial_{x_1}z)^2+(\partial_{x_2}z)^2+(\partial_{x_3}z)^2}{\chi(z)}}\mathrm{d}x_1\mathrm{d}x_2\mathrm{d}x_3. \tag{30}$$

It should be noted that, in this case, we denote the determinant of the reduced metric on surface $m(A)$ by h. Moreover, using the symmetry of region A and the bulk time slice, it can be determined that the minimal surface should have the same symmetry with A and can be defined by $z=z(x_1)$ as shown in Fig. 3. We then obtain the area of $m(A)$

$$\begin{aligned}\text{Area}(m(A))&=\int_A\frac{\mathrm{e}^{3A_e(z)}}{z^3}\sqrt{1+\frac{(\partial_{x_1}z)^2}{\chi(z)}}\mathrm{d}x_1\mathrm{d}x_2\mathrm{d}x_3\\&=M_1M_2\int_{-\frac{a}{2}}^{\frac{a}{2}}\frac{\mathrm{e}^{3A_e(z)}}{z^3}\sqrt{1+\frac{(\partial_{x_1}z)^2}{\chi(z)}}\mathrm{d}x_1,\end{aligned} \tag{31}$$

where M_1 and M_2 are the lengths of region A along the x_2 and x_3 directions, respectively. The minimal area equation can then be expressed as

$$\partial_{x_1}^2 z-\frac{3(z\partial_z A_e(z)-1)\left[\chi(z)+(\partial_{x_1}z)^2\right]}{z}-\frac{\partial_z\chi(z)(\partial_{x_1}z)^2}{2\chi(z)}=0. \tag{32}$$

We can then solve this minimal area equation using the following boundary conditions:

$$z(a/2)=0, \quad z(-a/2)=0, \tag{33}$$

or equally

$$z(a/2)=0, \quad \partial_{x_1}z(x_1)|_{x_1=0}=0. \tag{34}$$

Pluging the solution of the minimal area equation $z=z_m(x_1)$ into the area formula, we obtain the area of the minimal surface γ_A

$$\text{Area}(\gamma_A)=2M_1M_2\int_0^{\frac{a}{2}}\frac{\mathrm{e}^{3A_e(z_m)}}{z_m^3}\sqrt{1+\frac{(\partial_{x_1}z_m)^2}{\chi(z_m)}}\mathrm{d}x_1. \tag{35}$$

The holographic entanglement entropy for a strip shaped region is given as

$$\begin{aligned}S_A^{st}&=\frac{2\pi}{\kappa^2}\text{Area}(\gamma_A)\\&=\frac{4\pi M_1M_2}{\kappa^2}\int_0^{\frac{a}{2}}\frac{\mathrm{e}^{3A_e(z_m)}}{z_m^3}\sqrt{1+\frac{(\partial_{x_1}z_m)^2}{\chi(z_m)}}\mathrm{d}x_1.\end{aligned} \tag{36}$$

B. Numerical results

In this section, we first provide the numerical results for the black hole entropy of the holographic QCD model; then, we show the numerical results for the holographic entanglement entropy of a spherical shaped region and a strip shaped region.

1. *The black hole entropy*

Before we show the entanglement entropy on the QCD phase diagram, we first calculate the black hole entropy for different temperatures, T, and the baryon chemical potential, μ. We initially fix the constant $\kappa^2=1$ in the following calculation. In this case, we choose the divergent term to be

$$\int_{-\infty}^{\infty}\mathrm{d}x_1\int_{-\infty}^{\infty}\mathrm{d}x_2\int_{-\infty}^{\infty}\mathrm{d}x_3\to 0.11\ \text{GeV}^{-3}, \tag{37}$$

and note that we can fix this term to be any constant in principle. Then, the black hole entropy S_{bh} for a fixed μ as a function of the temperature is shown in Fig. 4.

The blue solid line is the physical value of S_{bh}/T^3. For the first order phase transition, the green dashed line does not physically correspond to the metastable state determined by the maximum of the free energy [33]. It is observed that at different chemical potentials, the black hole entropy, S_{bh}, or equally, S_{bh}/T^3 , is almost zero in

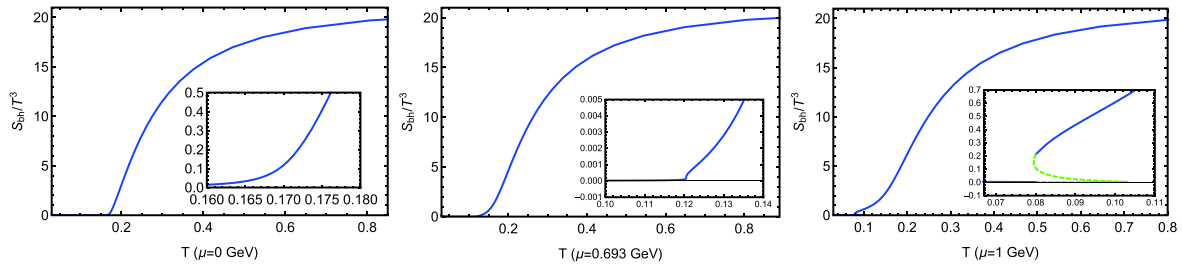

Fig. 4. (color online) The scaled black hole entropy S_{bh}/T^3 as a function of temperature for different quark chemical potentials. The blue solid lines are the physical black hole entropy from the minimal of the free energy. At $\mu=0$, phase transition occurs at $T=0.17$ GeV, and it is a crossover, so S_{bh} is single valued and smooth. When $\mu=0.693$ GeV, it is the critical endpoint of the first order phase transition and the transition temperature is $T=0.121$ GeV , whereS_{bh} is single valued but not smooth. For $\mu=1$ GeV, the first order phase transition occurs at $T=0.08$ GeV for which S_{bh} is not single valued, and the physical value of S_{bh} is not continuous at this point.

the hadron phase and then sharply increases at the phase boundary. At a very high temperature, the ratio of S_{bh}/T^3 has a constant value of approximately 20 for all temperatures. We then focus on the behavior of the black hole entropy at the phase boundary. It is determined that in the crossover region ($0\leqslant\mu<0.693$ GeV), the ratio of S_{bh}/T^3 is single valued and smooth. At the CEP ($\mu^E=0.693$ GeV, $T^E=0.121$ GeV), the ratio of S_{bh}/T^3 is single valued but not smooth. Moreover, in the first order phase transition region ($0.693\text{ GeV}<\mu$), the ratio of S_{bh}/T^3 is not single valued, which means that the ratio of S_{bh}/T^3 is not continuous at the first order phase boundary. As such, the black hole entropy or the normalized black hole entropy is simply the holographic duality of the entropy of thermal QCD.

2. *The holographic entanglement entropy*

In what follows, we will perform numerical calculation of the holographic entanglement entropy for a spherical shaped region and a strip shaped region. It should be noted that to obtain a finite area of the minimal surface, we also need to choose a UV-cutoff because of the boundary UV-divergence at $z=0\,\text{GeV}^{-1}$, which is called the renormalization of the holographic entanglement entropy [15, 16].

Firstly, we take the UV-cutoff to be $z=\epsilon$, and the area of minimal surface for a spherical shaped region and the strip shaped region are given as

$$S_A^{sp}=\frac{8\pi^2}{\kappa^2}\int_0^{r_0-\epsilon_0}r^2\mathrm{d}r\frac{\mathrm{e}^{3A_e(z_m)}}{z_m^3}\sqrt{1+\frac{(\partial_r z_m)^2}{\chi(z_m)}}, \tag{38}$$

$$\begin{aligned}S_A^{st}&=\frac{2\pi}{\kappa^2}\text{Area}(\gamma_A)\\&=\frac{4\pi M_1M_2}{\kappa^2}\int_0^{\frac{a}{2}-\epsilon_0}\frac{\mathrm{e}^{3A_e(z_m)}}{z_m^3}\sqrt{1+\frac{(\partial_{x_1}z_m)^2}{\chi(z_m)}}\mathrm{d}x_1.\end{aligned} \tag{39}$$

We choose $\epsilon=0.01\,\text{GeV}^{-1}$ in our calculation, and therefore, ϵ_0 is not a constant but a function of temperature T and the quark chemical potential μ , e.g., $\epsilon_0=\epsilon_0(T,\mu)$ as shown in Fig. 5.

Every minimal surface for different T and μ ends at the same point on the boundary with $z=0\ \text{GeV}^{-1}$. After taking the UV-cutoff, different surfaces have different boundaries on the slice of $z=0.01\,\text{GeV}^{-1}$. For the strip shaped region A, we also need to consider the parameters M_1 and M_2 to be finite, and we choose $M_1=M_2=1$ and $r_0=a/2=0.25\,\text{GeV}^{-1}$. Then, within the holographic QCD model and using the holographic entanglement entropy formulae Eqs. (38) and (39), we can calculate the holographic entanglement entropy between the two subregions A and $\bar{A}$ for different temperatures T and baryon chemical potentials μ. Fig. 6 shows the 3D-plot of the holographic entanglement entropy on the (T,μ) plane and the 2D-plot along the fixed baryon chemical potential line. It should be noted that the physical entanglement entropy could be determined from the minimal value of the free energy.

From Fig. 6, it is evident that the holographic entanglement entropies of a spherical shaped region, S_A^{sp}, and the strip shaped region, S_A^{st}, are very similar on the (T,μ) phase diagram. In the crossover region, both S_A^{sp} and S_A^{st} decrease initially at a low temperature, then increase, and then decrease again. Thus, a weak peak structure is formed around the phase boundary, which then increases sequentially in the QGP phase. However, it should be noted that although S_A^{sp} and S_A^{st} have very similar increasing and decreasing behavior on the phase diagram, they have different values for fixed T and μ. Near the phase boundary,S_A^{sp} and S_A^{st} change smoothly in the crossover region and form a weak peak structure in the vicinity of the phase boundary. However, we find that the top of the peak is not exactly the phase boundary. At CEP ($\mu^E=0.693$ GeV $T^E=0.121$ GeV), S_A^{sp} and S_A^{st} are continuous but not smooth. In addition, it should be noted that the CEP is exactly at the top of the peak in the vicinity of the phase boundary. In the first order phase trans-

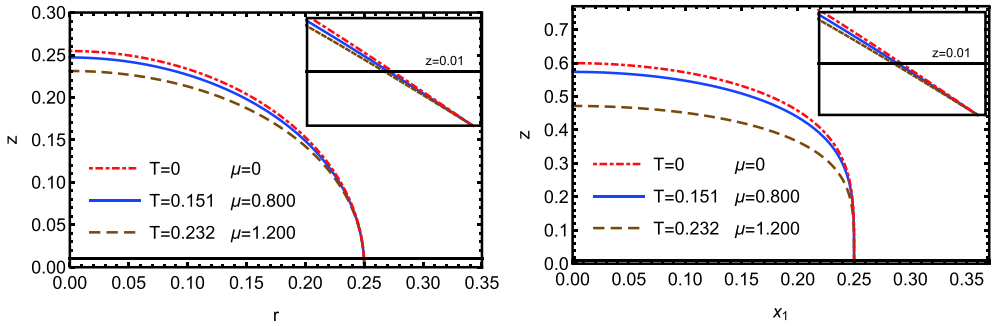

Fig. 5. (color online) The minimal surface with a UV-cutoff at $z = 0.01$ GeV^{-1} for different temperatures and baryon chemical potentials. (Left) The minimal surface for a spherical shaped region A. (Right) The minimal surface for a strip shaped region A. In this case, the unit for the temperature and the chemical potential μ is GeV.

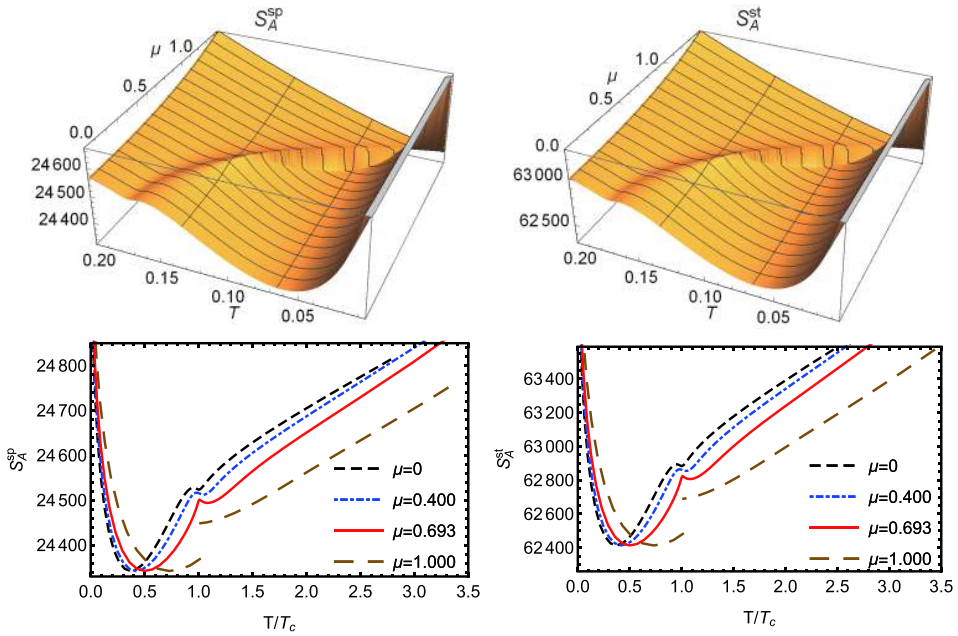

Fig. 6. (color online) 3D-plot of the holographic entanglement entropy on the (T,μ) plane and the 2D-plot along the fixed baryon chemical potential line. The unit for the temperature T and the chemical potential μ is GeV.

ition region, S_A^{sp} and S_A^{st} are not continuous at the phase boundary. These continuity properties are very similar to the case of the black hole entropy S_{bh}, and therefore, the holographic entanglement entropy of different boundary regions could also be a signal of QCD phase transition. However, it should be noted that several investigations [17, 18] have revealed a model dependence on the behavior of entanglement entropy in the phase diagram. Therefore, it is difficult provide a robust theoretical interpretation of this behavior of the entanglement entropy. However, despite the model dependence, it is evident that the behavior of entanglement entropy in the phase diagram is sensitive to the phase transition of quark matter.

3. *High temperature behavior*

In section III B.1, we concluded that the black hole entropy is the holographic duality of the thermal entropy of the QCD. Lattice results [34] show that the thermal entropy S_{th} has the behavior $S_{th} \sim T^3$ at high temperatures with $\mu = 0$. It is evident that the black hole entropy, S_{bh}, has the same property but the holographic entanglement entropy does not. At high temperatures, the behavior of holographic entanglement entropy is most likely to be proportional to T with $\mu = 0$ as shown in Fig. 7.

The black hole entropy, S_{bh}/T^3, represented as the solid line in the left figure matches the lattice result for the thermal entropy, S_{th}/T^3, and they both assume constant values. The holographic entanglement entropy for both regions is proportional to T at high temperatures when $\mu = 0$.

IV. OTHER ENTANGLEMENT PROPERTIES

The entanglement entropy measures the strength of

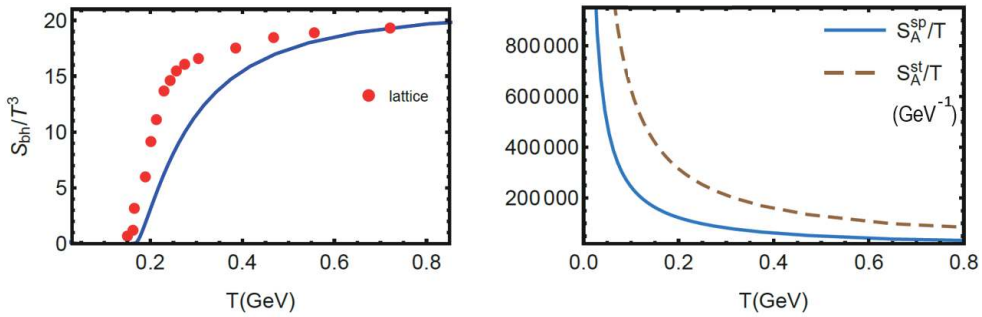

Fig. 7. (color online) The behavior of black hole entropy and entanglement entropy at high temperatures with $\mu=0$. (Left) The red dots are the lattice data [34] of thermal entropy, and the blue solid line is the black hole entropy in our holographic QCD model. (Right) S_A^{sp}/T and S_A^{st}/T at $\mu=0$.

the entanglement between different subsystems when the entire system is in a pure state. However, for a thermal state system, the entanglement entropy includes the contributions of the thermodynamics and not only the entanglement contributions. From the inequalities of entanglement entropy such as the subadditivity and the strong subadditivity, one can define other entanglement quantities. The two most often encountered quantities are called mutual information $MI(A,B)$ (5) and conditional mutual information $CMI(A,B|C)$ (6) [15, 16]. Another useful entanglement quantity for the study of entanglement property in a thermal system is the entanglement of purification (8) and its holographic duality, the entanglement wedge cross section (9) [27, 28].

In this section we only consider the strip shaped regions A and B defined as $a\leqslant x_1\leqslant b$ and $-\infty<x_i<\infty$. If we fix their boundaries a and b , the regions will be defined. The three situations of A and B that are considered are shown in Table 1.

A. Mutual information

In this section, we consider the mutual information of two unintersected subsystems A and B as shown in Fig. 8.

Mutual information $MI(A,B)$ is defined as follows:

$$MI(A,B)=S(A)+S(B)-S(AB). \tag{40}$$

We choose three nontrivial constructions of A and B as shown in Table 1, such that $MI(A,B)>0$ for any temperature T and baryon chemical potential μ. The holographic mutual information can then be calculated as

$$\begin{aligned} MI(A,B)=&S(A)+S(B)-S(AB)\\ =&\frac{1}{4G_N}[\text{Area}(\Sigma_{\text{gre}})-\text{Area}(\Sigma_{\text{red}})], \end{aligned} \tag{41}$$

where $\text{Area}(\Sigma_{\text{gre}})$ ($\text{Area}(\Sigma_{\text{red}})$) denotes the area of the green (red) surfaces as shown in Fig. 8. It should be noted that the green surfaces are the R-T surfaces of A and B,

Table 1. Three situations for the two subregions A and B used in this section. It should be noted that, for each subregion, we need to fix the two boundaries a and b that are shown in the second and third column (subregion A) or fourth and fifth column (subregion B) in the third to fifth row of Table 1.

Interval	A		B	
	a	b	a	b
1	−0.5	0.2	0.3	0.5
2	−0.5	0.1	0.2	0.5
3	−0.5	−0.05	0.05	0.5

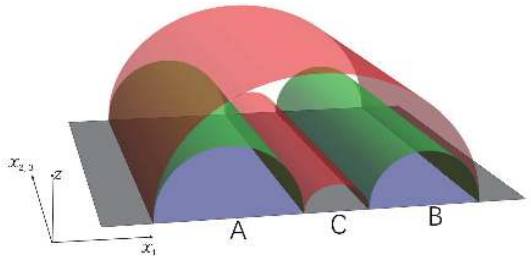

Fig. 8. (color online) Mutual information. The green surfaces are the R-T surfaces of A and B, and the red surfaces are the R-T surfaces of $A\cup B$.

and the red surfaces correspond to the R-T surfaces of $A\cup B$. The numerical results of mutual information for different settings of A and B are shown in Fig. 9.

We denote the mutual information $MI(A,B)$ of the three cases of A and B considered in Table 1 as MI-1, MI-2 and MI-3 correspondingly. The upper sub-figure of Fig. 9 shows the 3D-plot of the mutual information between A and B on the (T, μ) phase diagram. It is evident that $MI(A,B)$ for different constructions of A and B behaves similarly on the phase diagram if we ignore its exact values but exhibits different behaviors for the entanglement entropy, as shown in Fig. 6. $MI(A,B)$ does not change significantly in the hadron matter phase but increases with the increase in T and μ in the QGP phase. Similar to the entanglement entropy, in the crossover region,

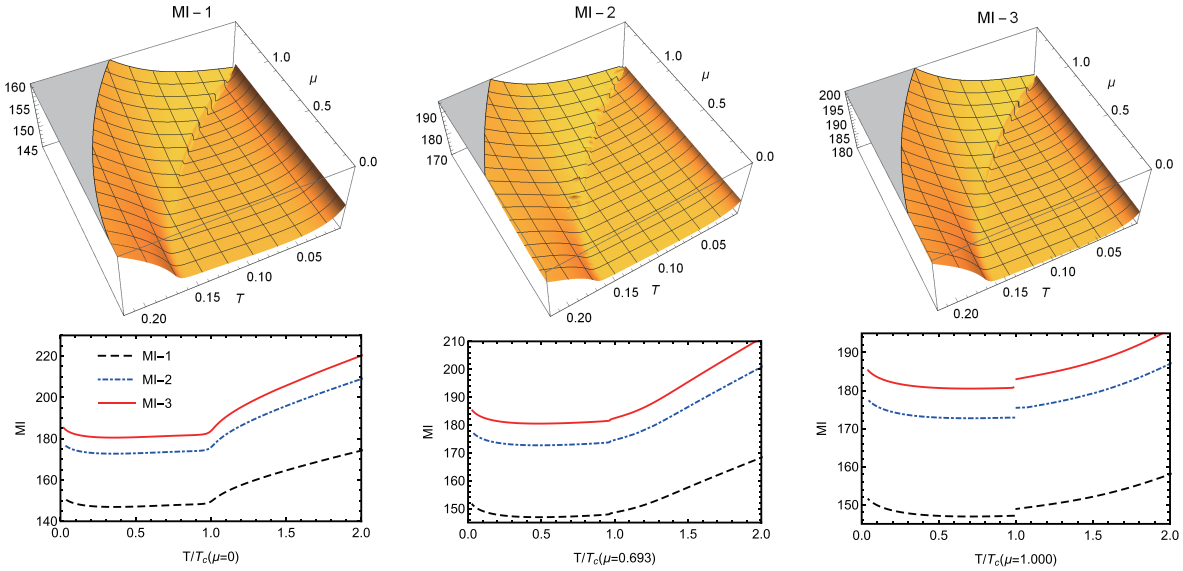

Fig. 9. (color online) (Upper) 3D-plot of the mutual information on the(T,μ) plane and (Lower) the 2D-plot along the fixed baryon chemical potential line for cases 1, 2, and 3 of A and B in Table 1. The unit for the temperature T and the chemical potential μ is GeV.

$MI(A,B)$ is single valued and changes smoothly near the phase boundary. It is continuous but not smooth at the CEP and is not single valued (and so is not continuous) at the first order phase boundary. Not surprisingly, $MI(A,B)$ is finite at any T and μ, although $S(A)$, $S(B)$, and $S(AB)$ are divergent. The lower 2D-plot in Fig. 9 shows the same result. However, the 2D-plot gives another interesting result

$$\text{MI}-1 \leqslant \text{MI}-2 \leqslant \text{MI}-3. \tag{42}$$

Considering the symmetry of the bulk spacetime, we have $\text{Area}(\Sigma^1_{\text{red}}) = \text{Area}(\Sigma^2_{\text{red}}) = \text{Area}(\Sigma^3_{\text{red}})$. In this case, the superscripts represent the corresponding three cases of A and B. Thus, this inequality implies that $S(A)+S(B)$ decreases with the increase in $|\text{Area}(A)-\text{Area}(B)|$ when $\text{Area}(A)+\text{Area}(B)$ is a constant. $\text{Area}(A)$ and $\text{Area}(B)$ denote the area of subregion A and B, respectively. When $\text{Area}(A)=\text{Area}(B)$, $S(A)+S(B)$ assumes the maximal value.

B. Conditional mutual information

In this section, we consider the conditional mutual information of two unintersected subsystems A and B as shown in Fig. 10.

The conditional mutual information is defined as

$$CMI(A,B|C) = S(AC)+S(BC)-S(ABC)-S(C). \tag{43}$$

The holographic mutual information can then be calculated as

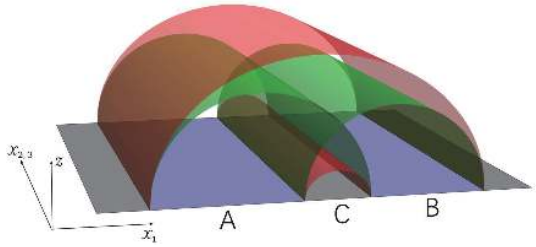

Fig. 10. (color online) Conditional mutual information. The green surfaces are the R-T surfaces of $A\cup C$ and $B\cup C$, and the red surfaces are the R-T surfaces of C and $A\cup B\cup C$.

$$\begin{aligned} CMI(A,B|C) =& S(AC)+S(BC)-S(ABC)-S(C) \\ =& \frac{1}{4G_N}[\text{Area}(\Sigma_{\text{gre}})-\text{Area}(\Sigma_{\text{red}})], \end{aligned} \tag{44}$$

where $\text{Area}(\Sigma_{\text{gre}})$ ($\text{Area}(\Sigma_{\text{red}})$) represents the area of the green (red) surfaces as shown in Fig. 10. The green surfaces are the R-T surfaces of $A\cup C$ and $B\cup C$, and the red surfaces correspond to the R-T surfaces of $A\cup B\cup C$ and C.

For the conditional mutual information, we also consider the same regions A and B as given in Table 1. Fig. 11 shows the 3D-plot of $CMI(A,B|C)$ on the (T, μ) phase diagram and its 2D-plot along a fixed μ.

It should be noted that similar to the case of mutual information, we also denote the three settings of A and B as CMI-1, CMI-2, and CMI-3. For different A, B, and C, $CMI(A,B|C)$ also behaves similarly on the (T, μ) phase diagram but has different values. Moreover, the behavior of $CMI(A,B|C)$ is very similar to that of $MI(A,B)$. It does not change significantly in the hadronic matter phase but increases rapidly with the increase in T and μ in the QGP

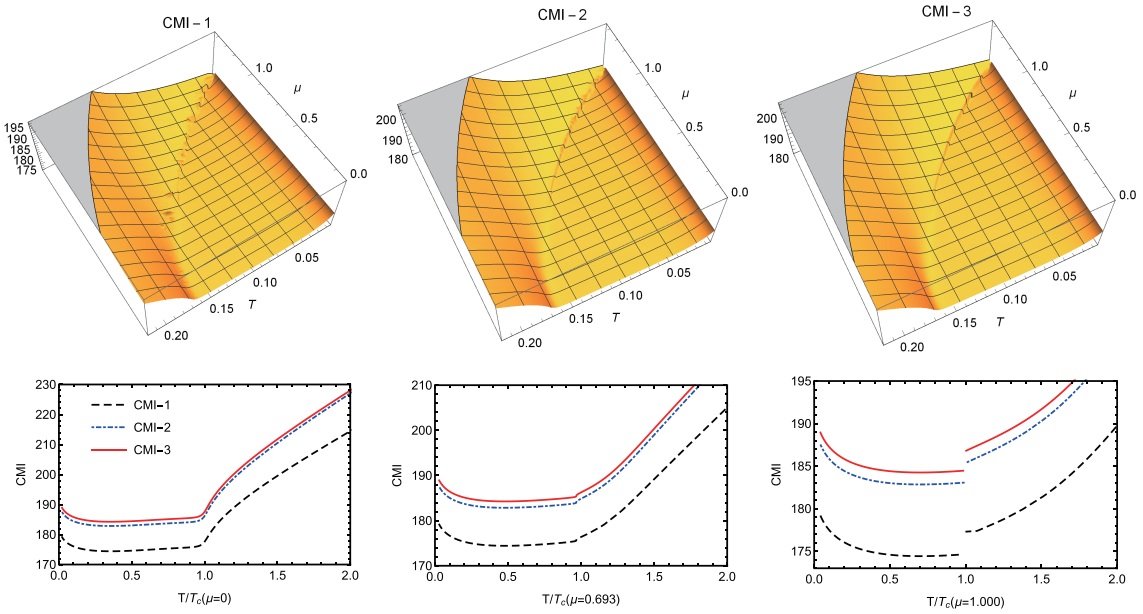

Fig. 11. (color online) (Upper) 3D-plot of the conditional mutual information on the (T,μ) plane and (Lower) the 2D-plot along a fixed baryon chemical potential line for cases 1, 2, and 3 of A and B in Table 1. The unit for temperature T and the chemical potential μ is GeV.

phase. Near the phase boundary, $CMI(A,B|C)$ changes smoothly in the crossover region and continuously but not smoothly at CEP; it exhibits discontinuous behavior in the first phase transition region. This implies that $CMI(A,B|C)$ could also be used to measure the entanglement between the subregions A and B, and it describes the phase transition of strongly coupled matter. The lower 2D-plot in Fig. 11 exhibits the same results and also yields a similar inequality

$$\text{CMI-1} \leqslant \text{CMI-2} \leqslant \text{CMI-3}. \tag{45}$$

Using the same argument in section IVA, firstly, considering the symmetry of the bulk spacetime, we have $\text{Area}(\Sigma^1_{\text{red}}) = \text{Area}(\Sigma^2_{\text{red}}) = \text{Area}(\Sigma^3_{\text{red}})$. The superscripts represent the three cases of A and B. Thus, the inequality implies that $S(AC)+S(BC)$ decreases with the increase in $|\text{Area}(A\cup C)-\text{Area}(B\cup C)|$ when $\text{Area}(A\cup C)+\text{Area}(B\cup C)$ is a constant; here, $\text{Area}(A\cup C)$ and $\text{Area}(B\cup C)$ correspond to the area of the subregions $A\cup C$ and $B\cup C$, respectively. When $\text{Area}(A\cup C)=\text{Area}(B\cup C)$, $S(AC)+S(BC)$ assumes the maximal value.

C. Entanglement of purification

In this section we consider the entanglement of purification of two unintersected subsystems A and B , as shown in Fig. 12. The holographic duality of entanglement of purification is the entanglement wedge cross section [27, 28]

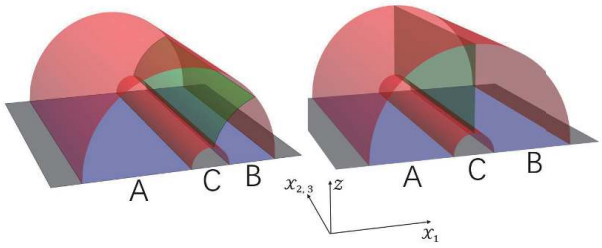

Fig. 12. (color online) The entanglement of purification. (Left) The asymmetry case and (Right) the symmetry case of A and B. The red surfaces are the R-T surfaces of $A\cup B$, and the green surface gives the minimal cross section of the entanglement wedge of A and B.

$$Ep(A,B) = Ew(A,B) = \frac{\text{Area}(\Sigma^{\min}_{AB})}{4G_N} = \frac{\text{Area}(\Sigma_{\text{gre}})}{4G_N}, \tag{46}$$

where $\text{Area}(\Sigma_{\text{gre}})$ represents the area of the green surfaces as shown in Fig. 12.

In this section, we only consider the symmetric case of A and B (case-3 in Table 1). The minimal surface is the surface with $x_1 = const$ as shown in the right sub-figure in Fig. 12. The asymmetric case of A and B is potentially much more complicated, and we may consider it in our next work. Fig. 13 shows the 3D-plot of $Ep(A,B)$ on the (T,μ) phase diagram and its 2D-plot along a fixed μ.

In [9], the authors propose that $Ew(A,B)$ could be equal to the mutual information if a group of bit flow related to the mutual information is introduced, which can be limited within the entanglement wedge and ends on A

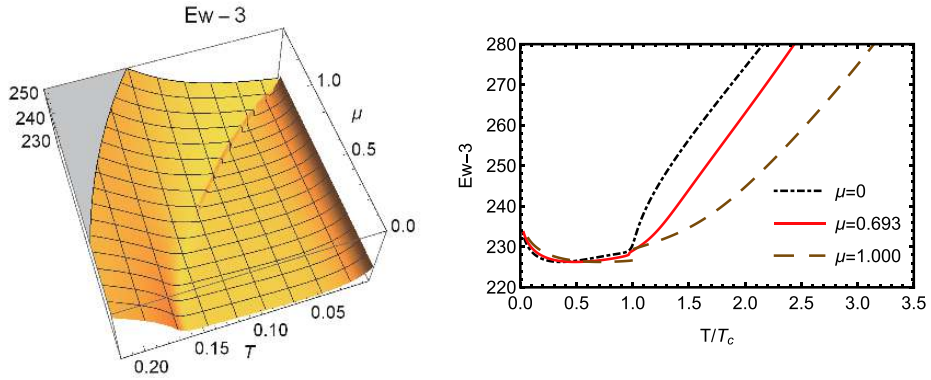

Fig. 13. (color online) (Left) 3D-plot of the entanglement of purification on the (T,μ) plane and (Right) the 2D-plot along a fixed baryon chemical potential line for case-3 of A and B in Table 1. The unit for the temperature T and the chemical potential μ is GeV.

and B. Moreover, in [27, 28] the authors suggested that $Ep(A,B)$ should be the holographic duality of the entanglement of purification of A and B. The 3D-plot in Fig. 13 shows a very similar behavior of $Ep(A,B)$ to $MI(A,B)$ and $CMI(A,B|C)$, as shown in Fig. 9 and Fig. 11. These similarities could also be observed in Fig. 14, where we plot the $MI(A,B)$ (red plot), $CMI(A,B|C)$ (green plot), and $Ep(A,B)-38$ (blue plot). It should be noted that, to compare these three entanglement quantities, we only consider the symmetric case of A and B (case-3 in Table 1). It is evident in Fig. 14 that for fixed T and μ $Ep(A,B)\geqslant CMI(A,B|C)\geqslant MI(A,B)$. The second "$\geqslant$" is due to the monogamy of the mutual information. If we consider the mutual information of A, B, and C, we have

$$\begin{aligned} I(A,B,C) =& S(A)+S(B)+S(C)-S(AB) \\ & -S(BC)-S(AC)+S(ABC) \\ =& -I(A,B|C)+I(A,B)\leqslant 0. \end{aligned} \tag{47}$$

The first "$\geqslant$" suggests that the maximal number of allowed bit threads that connect A and B is not equal to $MI(A,B)$ or $CMI(A,B|C)$.

V. CONCLUSION AND DISCUSSION

In this work, we investigated the holographic entanglement entropy of a holographic QCD model with a critical endpoint. We considered the behavior of entanglement entropy for a strip shaped region and a spherical shaped region on the phase diagram. It was determined that the behavior of holographic entanglement entropy on the phase diagram is independent of the shape of region A except for the exact value, although the minimal area equations for different A values are different. We also demonstrated how other entanglement quantities include mutual information, conditional mutual information, and the entanglement of purification behavior on the phase diagram. It was determined that the three entanglement quantities have very similar behavior: their values do not

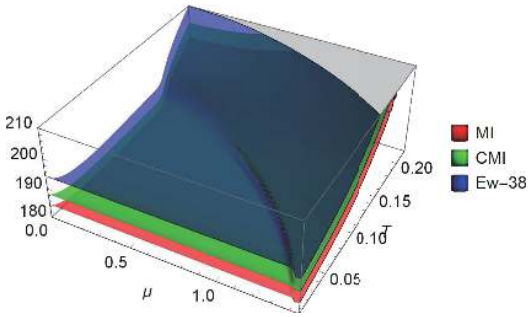

Fig. 14. (color online) The mutual information (MI), conditional mutual information (CMI), and entanglement of purification(Ew) for case-3 of A and B in Table 1.

change significantly in the hadronic matter phase but increases rapidly with the increase in T and μ in the QGP phase. Near the phase boundary, these three entanglement quantities change smoothly in the crossover region and continuously but not smoothly at CEP; they exhibit discontinuous behavior in the first phase transition region. Finally, we find an inequality for $Ep(A,B)$, $I(A,B|C)$ and $I(A,B)$

$$Ep(A,B)\geqslant CMI(A,B|C)\geqslant MI(A,B), \tag{48}$$

at any T and μ. This inequality suggests that the monogamy of $I(A,B,C)$ is still satisfied, and $Ep(A,B)$ is not the holographic duality of mutual information or conditional mutual information.

However, it should be noted that the black hole entropies for different holographic QCD models have a similar behavior. Even for $\mu=0$, the behavior of the holographic entanglement entropy does depend on the details of the hQCD models. For different hQCD models, the behavior of the holographic entanglement entropy on the (T, μ) phase diagram could be completely different. This indicates that the geometries of the bulk spacetime are completely different. In principle, the behavior of entanglement entropy between different subsystems of QCD matter should be unique. Therefore, the model dependence of

holographic entanglement entropy indicates that bulk geometry must be addressed. One approach is to utilize machine learning [35, 36]. An alternative method is to build a fully dynamic holographic QCD model. We are currently working on the latter.

ACKNOWLEDGEMENTS

We would like to thank Peng Liu for very helpful discussions.

References

[1] V. Neumann, *Mathematische Grundlagen der Quantenmechanik,* (Springer, Berlin, German), 1932

[2] J. M. Maldacena, *The Large N limit of superconformal field theories and supergravity,* Int. J. Theor. Phys. **38**, 1113–1133 (1999), arXiv: hep-th/9711200 [hep-th], [Adv. Theor. Math. Phys. **2**, 231 (1998)]

[3] S. Gubser, I. R. Klebanov, and A. M. Polyakov, Phys. Lett. B **428**, 105-114 (1998), arXiv:hep-th/9802109[hep-th]

[4] E. Witten, Adv. Theor. Math. Phys. **2**, 253-291 (1998), arXiv:hep-th/9802150[hep-th]

[5] O. Aharony, S. S. Gubser, J. M. Maldacena *et al*., Phys. Rept. **323**, 183-386 (2000), arXiv:hep-th/9905111[hep-th]

[6] M. Van Raamsdonk, *Building up spacetime with quantum entanglement*, Gen. Rel. Grav. **42**, 2323-2329 (2010), arXiv: 1005.3035 [hep-th], [Int. J. Mod. Phys. D **19**, 2429 (2010)]

[7] T. Faulkner, M. Guica, T. Hartman *et al*., JHEP **03**, 051 (2014), arXiv:1312.7856[hep-th]

[8] B. Swingle and M. Van Raamsdonk, *Universality of Gravity from Entanglement*, arXiv: 1405.2933 [hep-th]

[9] M. Freedman and M. Headrick, Commun. Math. Phys. **352**(1), 407-438 (2017), arXiv:1604.00354[hep-th]

[10] B. Czech, Phys. Rev. Lett. **120**(3), 031601 (2018), arXiv:1706.00965[hep-th]

[11] J. Erdmenger, N. Evans, I. Kirsch *et al*., Eur. Phys. J. A **35**, 81-133 (2008), arXiv:0711.4467[hep-th]

[12] G. F. de Teramond and S. J. Brodsky, *Hadronic Form Factor Models and Spectroscopy Within the Gauge/Gravity Correspondence,* in *Proceedings, Ferrara International School Niccolo Cabeo: Hadron Electromagnetic Form Factors: Ferrara, Italy, May 23-28, 2011*, pp. 54-109. 2011. arXiv: 1203.4025 [hep-ph], http://www-public.slac.stanford.edu/sciDoc/docMeta.aspx?slacPubNumber=SLAC-PUB-14860

[13] Y. Kim, I. J. Shin, and T. Tsukioka, Prog. Part. Nucl. Phys. **68**, 55-112 (2013), arXiv:1205.4852[hep-ph]

[14] A. Adams, L. D. Carr, T. Schafer *et al*., New J. Phys. **14**, 115009 (2012), arXiv:1205.5180[hep-th]

[15] S. Ryu and T. Takayanagi, Phys. Rev. Lett. **96**, 181602 (2006), arXiv:hep-th/0603001[hep-th]

[16] S. Ryu and T. Takayanagi, JHEP **0608**, 045 (2006), arXiv:hep-th/0605073[hep-th]

[17] S.-J. Zhang, Nucl. Phys. B **916**, 304-319 (2017), arXiv:1608.03072[hep-th]

[18] J. Knaute and B. Kampfer, Phys. Rev. D **96**(10), 106003 (2017), arXiv:1706.02647[hep-ph]

[19] M. Ali-Akbari and M. Lezgi, Phys. Rev. D **96**(8), 086014 (2017), arXiv:1706.04335[hep-th]

[20] D. Dudal and S. Mahapatra, JHEP **04**, 031 (2017), arXiv:1612.06248[hep-th]

[21] D. Dudal and S. Mahapatra, JHEP **07**, 120 (2018), arXiv:1805.02938[hep-th]

[22] S. Mahapatra, JHEP **04**, 137 (2019), arXiv:1903.05927[hep-th]

[23] X. Dong, Phys. Rev. Lett. **116**(25), 251602 (2016), arXiv:1602.08493[hep-th]

[24] L. Bianchi, S. Chapman, X. Dong *et al*., JHEP **11**, 180 (2016), arXiv:1607.07418[hep-th]

[25] G. Cavini, D. Seminara, J. Sisti *et al*., *On shape dependence of holographic entanglement entropy in AdS_4/CFT_3 with Lifshitz scaling and hyperscaling violation*, arXiv: 1907.10030 [hep-th]

[26] B. Chen, Z. Li, and J.-j. Zhang, JHEP **09**, 151 (2017), arXiv:1707.07354[hep-th]

[27] T. Takayanagi and K. Umemoto, Nature Phys. **14**(6), 573-577 (2018), arXiv:1708.09393[hep-th]

[28] P. Nguyen, T. Devakul, M. G. Halbasch *et al*., JHEP **01**, 098 (2018), arXiv:1709.07424[hep-th]

[29] P. Liu, Y. Ling, C. Niu *et al*., JHEP **09**, 071 (2019), arXiv:1902.02243[hep-th]

[30] Y.-f. Huang, Z.-j. Shi, C. Niu *et al*., *Mixed State Entanglement for Holographic Axion Model*, arXiv: 1911.10977 [hep-th]

[31] M. Ghodrati, X.-M. Kuang, B. Wang *et al*., JHEP **09**, 009 (2019), arXiv:1902.02475[hep-th]

[32] B. M. Terhal, M. Horodecki, D. W. Leung *et al*., J. Math. Phys. **43**, 4286 (2002), arXiv:quant-ph/0202044[quant-ph]

[33] Y. Yang and P.-H. Yuan, JHEP **11**, 149 (2014), arXiv:1406.1865[hep-th]

[34] F. Karsch, PoS **CPOD07**, 026 (2007), arXiv:0711.0656[hep-lat]

[35] K. Hashimoto, S. Sugishita, A. Tanaka *et al*., Phys. Rev. D **98**(4), 046019 (2018), arXiv:1802.08313[hep-th]

[36] K. Hashimoto, S. Sugishita, A. Tanaka *et al*., Phys. Rev. D **98**(10), 106014 (2018), arXiv:1809.10536[hep-th]